Advances in Energy and Materials Research https://jaem.qom.ac.ir/

Solid state synthesis, characterization and physical properties of CeO_2-$Dy_2Ce_2O_7$ nanocomposites

Shahin Khademinia

Department of Inorganic Chemistry, Faculty of Chemistry, University of Semnan, Semnan, Iran. Email: khademiniashahin@gmail.com

Article Info

Article type:
Research Article

Article history:
Received 27 Jan 2024
Received in revised form 12 May 2024
Accepted 9 Jul 2024
Published online 28 Sep 2024

Keywords:
$Dy_2Ce_2O_7$, Nanomaterial, Solid State Method, Characterization.

ABSTRACT

$Dy_2Ce_2O_7$ nanopowders were synthesized for the first time via solid-state reactions using $Ce(NO_3)_3·6H_2O$ and Dy_2O_3 as raw materials in a stoichiometric 1:1 Ce:Dy molar ratio. The synthesized materials were characterized by powder X-ray diffraction (PXRD). Structural analysis, performed using the FullProf program with profile matching and constant scale factors, confirmed a predominant cubic $Dy_2Ce_2O_7$ structure with the Fd-3m space group. Field-emission scanning electron microscopy (FESEM) revealed that the $Dy_2Ce_2O_7$ particles exhibited uniform spherical morphologies. Ultraviolet-visible (UV-Vis) spectroscopy demonstrated strong light absorption in the UV-visible region. The direct optical band gaps for samples S1, S2, S3, and S4 were determined to be 2.7 eV, 2.6 eV, 2.5 eV, and 2.4 eV, respectively.

Cite this article: Khademinia, S. (2025). Solid state synthesis, characterization and physical properties of CeO_2-$Dy_2Ce_2O_7$ nanocomposites, *Advances in Energy and Materials Research*, 2 (1), 1-5. https://doi.org/10.22091/jaem.2025.13072.1026

DOI: 10.22091/jaem.2025.13072.1026
Publisher: University of Qom.

1. Introduction

Oxides with general formula $A_2B_2O_8$ (where A is a medium – large cation and B is an octahedrally coordinated, high – charge cation) have been studied extensively. Pyrochlore materials with general formula $A_2B_2O_7$ are related to the fluorite structure and the nature of this relationship is discussed in the crystallography of the this compounds [1]. One of the most attractive and effective rare earth materials is rare earth-doped cerium oxide materials that have excellent and substantial mechanical, electrical, catalytic and optical characteristics. Rare earth-doped cerium oxide materials have received a particular attention owing to their usages in the solid oxide fuel cells (SOFC), oxygen sensors, catalyst carriers, photocatalyst and thermal barrier coatings [2-8]. Rare earth-doped cerium oxide has been synthesized through utilizing various routes including carbonate coprecipitation, citrate auto ignition, solid state reaction and combustion [9-14]. $Dy_2Ce_2O_7$ belongs to the family of the rare earth-doped cerium oxide materials. Since rare earth-doped cerium oxide materials have excellent and substantial electrical, optical, mechanical and catalytic characteristics, they have become one of the most attractive and important materials for oxygen sensors, photocatalyst, thermal barrier coatings, solid oxide fuel cells (SOFC) and catalyst carriers [15-21]. There is no report on the synthesis of the nanostructured $Dy_2Ce_2O_7$ by this method. Crystalline phase growth of the synthesized materials in different conditions was investigated using Rietveld analysis. Physical properties of the synthesized nanomaterials were studied using field emission scanning electron microscope (FESEM), ultraviolet visible (UV- Vis) spectroscopy.

2. Experimental

2.1. Materials and instruments

All chemicals including Dy_2O_3 and $Ce(NO_3)_3.6H_2O$ were of analytical grade and obtained from commercial sources (Merck Company) and used without further purifications. Phase identifications were performed on a powder X-ray diffractometer D5000 (Siemens AG, Munich, Germany) using CuK_α radiation. The Rietveld analysis was performed by *FullProf* software. The morphology of the obtained materials was examined with a field emission scanning electron microscope (Hitachi FE-SEM model S-4160). Absorption spectra were recorded on a UV-visible spectrophotometer model-UV-1650 PC (Shimadzu, Japan).

2.2. Solid State synthesis of $Dy_2Ce_2O_7$ nanomaterials

In a typical synthesis experiment, 0.186 g (0.5 mmol) of Dy_2O_3 (M_W = 373.0 g mol^{-1}) and 0.326 g (1 mmol) of Ce(NO3)3.6H2O (M_w = 326.13 g mol^{-1}) with Dy:Ce molar ratio of 1:1 were mixed in a mortar until an almost homogenous powder was obtained. The obtained powder was added into a 25 mL crucible and then transferred to an electric furnace that had already reached to a desired temperature at S_1 = 800℃, S_2 = 900℃, S_3 = 1000℃ (8 h) and S_4 = 1000℃ (10 h). The Crucible was then cooled normally in the furnace to the room temperature. The acquired powder was collected for further analyses.

3. Results and discussions

3.1. Characterization

The phase identification of the synthesized nanomaterials was performed by powder X-ray diffraction technique. Figure 1 shows the X-ray diffraction (XRD) analysis of the obtained samples in the 2θ range 10-90° as well as the structural analyses performed by the *FullProf* program. The structural analyses were performed employing profile matching with constant scale factors. Red lines are the observed intensities; the black ones are the calculated data; the blue ones are the difference: Yobs-Ycalc. The Bragg reflections positions are demonstrated by blue and red corresponded to cubic phases of $Dy_2Ce_2O_7$ and CeO_2, respectively. Figure 1 represents the PXRD patterns of the obtained $Dy_2Ce_2O_7$ nanomaterials. The data indicate that the PXRD patterns of the synthesized compounds at the reaction temperatures in the range from 800 to 1000 °C are related to cubic crystal structure. It is clear that the reaction temperature is a key factor affected the crystal phase composition. The results showed that the pattern had a main $Dy_2Ce_2O_7$ crystal structure with space group Fd-3m.

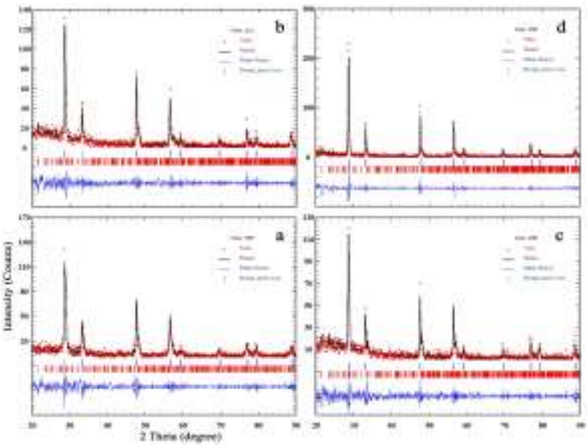

Figure 1. X-Ray diffraction patterns and the rietveld analyses of a) S_1, b) S_2, c) S_3 and d) S_4.

Table 1 shows the crystallite sizes of the synthesized nanomaterials in different reaction temperatures that were calculated by Scherrer equation (equation 1). In this equation, D is the entire thickness of the crystallite sample, λ is the X-ray diffraction wavelength (0.154 nm), and k is Scherrer constant (0.9), $B_{1/2}$ of FWHM is the full width at half of its maximum intensity and θ is the half diffraction angle at which the peak is located. Also, interplanar spacing in the crystalline material was measured by Bragg's law ($\boldsymbol{n\lambda = 2\mathrm{d}\sin(\theta)}$). The data mentioned in table 1 shows that with increasing the reaction temperature, $Dy_2Ce_2O_7$ purity is increased. It is clear that when the reaction temperature is increased, $Dy_2Ce_2O_7$ crystal phase stability of the material is decreased at high temperature.

$$\boldsymbol{D}\ (\mathrm{nm}) = K\lambda / B_{hkl} \cos\theta \qquad (1)$$

Table 1. Crystallite size data for $Dy_2Ce_2O_7$ nanomaterials.

Sample	2θ	B°	Brad	D	d	a=b=c	R_F	R_{Brag}	χ^2	Intensity	Purity
S_1	33.2262	0.28822	0.00503	29	2.7	5.38790	2.21	3.05	1.15	133	87
S_2	33.1569	0.23275	0.00406	35	2.7	5.39913	0.93	1.16	1.06	133	85
S_3	33.1269	0.23273	0.00406	35	2.7	5.40403	1.05	1.36	1.00	121	84
S_4	33.1759	0.23277	0.00406	35	2.7	5.39578	1.94	2.07	1.08	233	93

The crystallite sizes of the obtained targets were calculated by using equation 1 and choosing a peak at about 33.17° for $Dy_2Ce_2O_7$ nanomaterials. According to the table 1,the crystallite sizes were decreased by increasing the reaction temperature.

Table 1 indicates the lattice parameters data for $Dy_2Ce_2O_7$ calculated by Rietveld analysis. By increasing the reaction temperature, the cell parameters were increased. R_f, R_B and χ^2 values show the goodness of the fittings. The reaction temperature is the main factor on the crystal phase growth and the purity of the obtained materials. When the reaction time and temperature are increased to 1000 °C and 10 h, the phase purity of $Dy_2Ce_2O_7$ is increased (S_1-S_4).

3. 3. Morphology analysis

FESEM images of the synthesized $Dy_2Ce_2O_7$ nanomaterials are shown in figures 2. İt is obvious in figure 2 a that with increasing the reaction temperature to 800 °C (S_1) and 1000 °C (S_4) the morphology of the materials is particles (figure 2 d) and the minimum particles size is about 30 - 70 nm. The morphology of S_4 is large particle (figure 2d) with pourous structure. As a result, increasing the reaction temperature changes the morphology from sponge to plate, multigonal particles and large bulk particles.

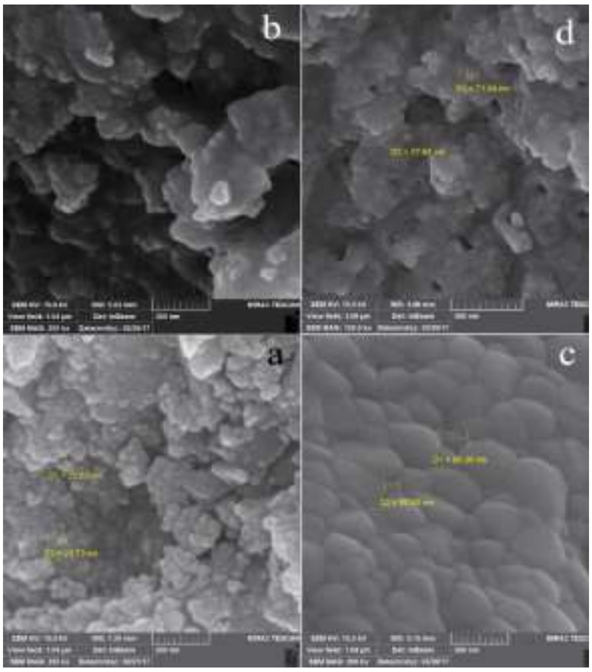

Figure 2. FESEM images of a) S_1, b) S_2, c) S_3 and d) S_4.

3.4. Optical properties

Figurs 3 and 4, respectively, shows the UV-Vis spectrum and band gap caculation data. The UV-Vis spectrum of $Dy_2Ce_2O_7$ in figure 8 respectively are shown. According to the results of Pascual et al.[22], the relation between the absorption coefficient and incident photon energy can be written as $(\alpha h\nu)^2 = A(h\nu - Eg)$, where A and Eg are a constant and the direct band gap energy, respectively. Band gap energies were evaluated from extrapolating the linear part of the curve to the energy axis. The band gap of $Dy_2Ce_2O_7$ nanomaterials obtained at $S_1 = 800$, $S_2 = 900$, $S_3 = 1000$ (8 h) and $S_4 = 1000$ (10 h), respectively, were 2.7 eV, 2.6 eV, 2.5 eV and 2.4 eV. The decreasing of the band gap energies could be attributed to the increasing the phase purity of the obtained materials in the fluorites phase. The band gap, absoption edge and reaction condition in different temperature and time of the synthesized materials are summarized in table 2.

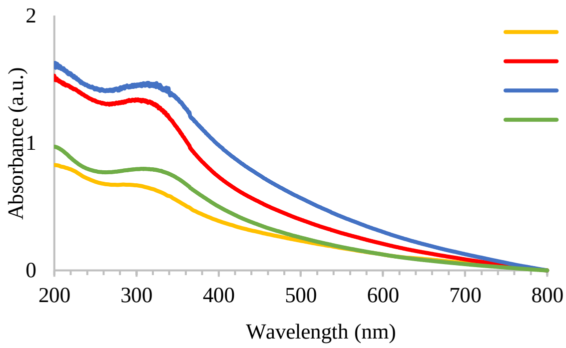

Figure 3. Plots of $(\alpha h\nu)^2$ versus hν for the synthesized samples.

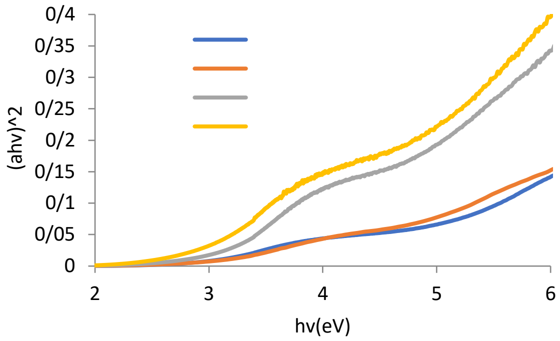

Figure 4. Plots of (a) UV-Vis spectrum for the synthesized samples.

Table 3. Band gap data and absorption edge for the obtained $Dy_2Ce_2O_7$ nanomaterials.

Property	S_1	S_2	S_3	S_4
Time (h)	8	8	8	10
Temperature (°C)	800	900	1000	1000
Band gap(eV)	2.7	2.6	2.5	2.4
absorption edge (nm)	480	500	510	520

4. Conclusion

In this work, Dy2Ce2O7 nanomaterials were synthesized successfully via solid state and hydrothermal method. PXRD analysis corroborate the successful synthesis of the mentioned material. The Rietveld analysis showed that the reaction temperature played an important effect on the phase purity and crystal growth. FESEM image indicate that the as-synthesized nanomaterial had a mixture of rod, sponge and circle morphologies. We understood that the reaction temperature and time has a main effect on the morphology of the nanomaterials obtained. UV- Vis spectra of the synthesized nanomaterial were investigated and band gap energies were calculated.

Conflict of Interest

The authors declare that there are no conflicts of interest.

Reference

[1] A.R. Cleave, Atomic scale simulations for waste form applications, in, University of London London, UK, 2006.

[2] J. S. Bae, W. K. Choo, Ch. H. Lee, The crystal structure of ionic conductor LaxCe1–xO2–x/2, J. Eur. Ceram. 24 (2004) 1291–1294. DOI: https://doi.org/10.1016/S0955-2219(03)00499-0

[3] Y. Wang, H. Guo, Sh. Gong, Thermal shock resistance and mechanical properties of La2Ce2O7 thermal barrier coatings with segmented structure, Ceram. Int. 35 (2009) 2639–2644. DOI: https://doi.org/10.1016/j.ceramint.2009.02.025

[4] W. M. O'Neill, M. A. Morris, The defect chemistry of lanthana–ceria mixed oxides by MASNMR, Chem. Phys. Lett. 305 (1999) 389–394. DOI: https://doi.org/10.1016/S0009-2614(99)00343-7

[5] V. Besikiotis, Ch. S. Knee, I. Ahmed, R. Haugsrud, T. Norby, Crystal structure, hydration and ionic conductivity of the inherently oxygen-deficient La2Ce2O7, Solid State Ionics 228 (2012) 1–7. DOI: https://doi.org/10.1016/j.ssi.2012.08.023

[6] E. Y. Pikalova, A. A. Murashkina, V. I. Maragou, A. K. Demin, V. N. Strekalovsky, P. E. Tsiakaras, CeO2 based materials doped with lanthanides for applications in intermediate temperature electrochemical devices, Int. J. Hydrogen Energy 36 (2011) 6175–6183. DOI: https://doi.org/10.1016/j.ijhydene.2011.01.132

[7] Ch. Wang, Y. Wang, A. Zhang, Y. Cheng, F. Chi, Zh. Yu, The influence of ionic radii on the grain growth and sintering-resistance of Ln2Ce2O7 (Ln 5 La, Nd, Sm, Gd), J. Mater. Sci. 48 (2013) 8133–8139. DOI: https://doi.org/10.1007/s10853-013-7625-x.

[8] S. Kuharuangrong, Ionic conductivity of Sm, Gd, Dy and Er-doped ceria, J. Power Sources 171 (2007) 506–510. DOI: https://doi.org/10.1016/j.jpowsour.2007.05.104

[9] J. J. G. Li, T. Ikegami, T. Mori, T. Wada, Reactive Ce0.8RE0.2O1.9 (RE = La, Nd, Sm, Gd, Dy, Y, Ho, Er, and Yb) Powders via Carbonate Coprecipitation, Chem. Mater. 13 (2001) 2913–2920. DOI: https://doi.org/10.1021/cm010148x

[10] A. K. Baral, V. Sankaranarayanan, Ionic Transport Properties in Nanocrystalline Ce0.8A0.2O2-δ (with A = Eu, Gd, Dy, and Ho) Materials, Nanoscale. Res. Lett. 5 (2010) 637–643. DOI: https://doi.org/10.1007/s11671-010-9527-z

[11] Y. Y. P. Fu, S. H. Chen, F. Y. Tsai, Sh. H. Hu, Aqueous tape casting and crystallization kinetics of Ce0.8La0.2O1.9 powder, Ceram. Int. 35 (2009) 609–615. DOI: https://doi.org/10.1016/j.ceramint.2008.01.018

[12] Zh. Zhu, L. Yan, H. Liu, W. Sun, Q. Zhang, W. Liu, A mixed electronic and protonic conducting hydrogen separation membrane with asymmetric structure, Int. J. Hydrogen Energy 37 (2012) 12708–12713. DOI: https://doi.org/10.1016/j.ijhydene.2012.06.033

[13] H. Zhang, S. Liao, X. Dang, Sh. Guan, Zh. Zhang, Preparation and thermal conductivities of Gd2Ce2O7 and (Gd0.9Ca0.1)2Ce2O6.9 ceramics for thermal barrier coatings, J. Alloys Compd. 509 (2011) 1226–1230. DOI: https://doi.org/10.1016/j.jallcom.2010.09.196.

[14] W. Sun, S. Fang, L. Yan, W. Liu, Investigation on Proton Conductivity of La2Ce2O7 in Wet Atmosphere: Dependence on Water Vapor Partial Pressure, Fuel Cells 12 (2012) 457–463. DOI: https://doi.org/10.1002/fuce.201100175.

[15] Y. Wang, H. Guo, Sh. Gong, Ceram. Int., 2009, 35, 2639. DOI: https://doi.org/10.1016/j.ceramint.2009.02.025

[16] W.M O'Neill, M.A Morris, Chem. Phys. Lett., 1999, 305, 389. DOI: https://doi.org/10.1016/S0009-2614(99)00343-7

[17] J.S. Bae, W.K. Choo, Ch.H. Lee, J. Eur. Ceram. Soc., 2004, 24, 1291. DOI: https://doi.org/10.1016/S0955-2219(03)00499-0

[18] V. Besikiotis, Ch. S. Knee, I. Ahmed, R. Haugsrud, T. Norby, Solid State Ionics, 2012, 228, 1. DOI: https://doi.org/10.1016/j.ssi.2012.08.023

[19] Ch. Wang, Y. Wang, A. Zhang, Y. Cheng, F. Chi, Zh. Yu, J. Mater. Sci., 2013, 48, 8133. DOI: https://doi.org/10.1007/s10853-013-7625-x

[20] E.Y. Pikalova, A.A. Murashkina, V.I. Maragou, A.K. Demin, V.N. Strekalovsky, P.E. Tsiakaras, Int. J. Hydrogen Energy, 2011, 36, 6175. DOI: https://doi.org/10.1016/j.ijhydene.2011.01.132
[21] S. Kuharuangrong, J. Power Sources, 2007, 171, 506. DOI: https://doi.org/10.1016/j.jpowsour.2007.05.104
[22] J. Pascual, J. Camassel, H. Mathieu, Fine structure in the intrinsic absorption edge of Ti O 2, Physical Review B, 18 (1978) 5606. DOI: https://doi.org/10.1103/PhysRevB.18.5606